**Biogeosciences
Discussions**

Biogeosciences Discussions is the access reviewed discussion forum of *Biogeosciences*

**Bacteriogenic iron
oxides**

L. Corbari et al.

Iron oxide deposits associated with the ectosymbiotic bacteria in the hydrothermal vent shrimp Rimicaris exoculata

L. Corbari[1], M.-A. Cambon-Bonavita[2], G. J. Long[3], F. Grandjean[4], M. Zbinden[5],
F. Gaill[5], and P. Compère[1]

[1]Université de Liège, Laboratoire de Morphologie fonctionnelle et évolutive, Unité de
Morphologie ultrastructurale et Cellule d'Appui Technologique en Microscopie (Catμ), allée de
la chimie, 3, 4000 Liège, Belgium
[2]Laboratoire de Microbiologie et Biotechnologie des Extrêmophiles, Ifremer, centre de Brest,
BP 70, 29280 Plouzané, France
[3]Department of Chemistry, Missouri University of Science and Technology, University of
Missouri-Rolla, Rolla, Missouri 65409-0010, USA

[4]Department of Physics, B5, University of Liège, 4000 Sart-Tilman, Belgium

[5]UMR CNRS 7138 "Systématique, Adaptation et Evolution", Université Pierre et Marie Curie, 7 Quai St Bernard, Bâtiment A, 75252 Paris Cedex 05, France

Correspondence to: L. Corbari (lcorbari@ulg.ac.be)

Bacteriogenic iron oxides

L. Corbari et al.

Full Screen / Esc

Title Page

| Abstract | Introduction |

| Conclusions | References |

| Tables | Figures |

| ◀◀ | ▶▶ |

| ◀ | ▶ |

| Back | Close |

Full Screen / Esc

Abstract

The *Rimicaris exoculata* shrimp is considered a primary consumer that dominates the fauna of most Mid-Atlantic Ridge (MAR) hydrothermal ecosystems. These shrimps harbour in their gill chambers an important ectosymbiotic community of chemoau-
5 totrophic bacteria associated with iron oxide deposits. The structure and elemental composition of the minerals associated with these bacteria have been investigated by using X-ray microanalyses, light microscopy, and transmission, environmental scanning and scanning transmission electron microscopy. The nature of the iron oxides in shrimps obtained from the Rainbow vent field at 36°14.0′ N, has also been deter-
10 mined by Mössbauer spectroscopy. This multidisciplinary approach has revealed that the three step-levels of mineral crust found in the *Rimicaris exoculata* shrimps consist of heavy concretions formed by nanoparticles of two-line ferrihydrite intermixed with minor inorganic SiO_2, $(Ca,Mg)SO_4$, and $(Ca,Mg)_3(PO4)_2$ minerals that may stabilise the ferrihydrite form of iron oxides. Morphological observations on the bacteria have
15 revealed their close interactions with these minerals and, thus, indicate the biogenic origin of the iron oxide deposits. The evolution of the bacterial density in the three mineral crust levels is related to the amount of the iron deposits and it is proposed that the lower crust level is the most likely region for the location of the iron-oxidizing bacteria.

1 Introduction

20 *Rimicaris exoculata* (Williams and Rona, 1986) is one of the most dominant species found at the Mid-Atlantic Ridge (MAR) hydrothermal vents. This endemic shrimp swarms on the chimney walls, exhibiting a patch-like distribution of up to several thousand per square meter (Segonzac et al., 1993). In extreme deep-sea environments, such high population density levels require some specific adaptations. Many hydrother-
25 mal organisms derive their nutrition from chemoautotrophic bacteria through symbioses relying most often on sulphide or methane as an energy source (Cavanaugh,

2006). *R. exoculata* possess an original ectosymbiotic bacterial community, housed in its expanded gill chambers and mouth parts (Van Dover et al., 1988; Casanova et al., 1993; Zbinden et al., 2004; Corbari et al., 2008). Even though numerous authors have suggested that, if really ectosymbiotic, the bacteria could be a direct or indirect food source for the shrimp (Segonzac et al., 1993; Rieley et al., 1999; Gebruk et al., 2000; Zbinden et al., 2004). Still undetermined, however, is the origin of the nutritional carbon of *R. exoculata* and the role of the bacterial ectosymbiosis play as a trophic resource (Pond et al., 1997; Polz et al., 1998; Zbinden and Cambon-Bonavita, 2003). The bacterial community housed in the gill chamber of *R. exoculata* has been identified as chemoautotrophic bacteria (Wirsen et al., 1993) and phylogenetic analysis revealed that the bacteria could correspond to a single epsilon-proteobacteria phylotype (Polz and Cavanaugh, 1995). Some authors have also hypothesized that the bacteria could acquire their energy from sulphide oxidation (Gebruk et al., 1993; Polz and Cavanaugh, 1995), but this hypothesis has never been confirmed by any culture experiment.

In the absence of cultivated bacteria, recent studies have focussed on the description of both the bacteria and the mineral deposits in *R. exoculata*. Zbinden et al. (2004) described three bacterial morphotypes, individual rods with an approximate size of $0.5 \times 1.5\,\mu$m, and two types of multicellular filaments, i.e., thick filaments with 2 to $3\,\mu$m diameters and thin filaments with 0.5 to $1\,\mu$m diameters, found within the entire gill chamber. They mapped the location of these bacteria and divided their associated minerals into three functional compartments, that which were considered to represent distinct microenvironments. One of these compartments, the upper pre-branchial chamber, houses the highest density of both bacteria and minerals. A recent study (Corbari et al., 2008) focussed on this compartment and delineated the shrimp-bacteria-mineral association throughout the shrimp moult cycle. This study performed on about 300 specimens from two vent sites, TAG and Rainbow, indicated that the bacterial community restarts after each exuviation and gradually colonises the gill chamber in five moult stage-correlated steps. Moreover, the presence of red-brown mineral deposits in the gill chamber, including the mouth parts and branchiostegites, of the *R. exoculata* has

already been described (Gloter et al., 2004; Zbinden et al., 2004). These deposits have been identified as hydrous iron oxide in the form of ferrihydrite (Gloter et al., 2004). The extent and density of iron oxide deposits within the gill chamber are both responsible for the external colour of the shrimp, a colour that may be macroscopically observed by
5   transparency through the branchiostegites (Zbinden et al., 2004). The shrimp external colour ranges from white, indicative of no mineral deposits, to dark-red, indicative of a heavily mineralised crust; the colour appears to be highly correlated with the moult stages (Corbari et al., 2008). The fully-formed mineral crust is roughly organised in three step-levels that illustrate the time-related formation and growth of the mineral
10 particles (Corbari et al., 2008). The shrimp-bacteria ectosymbiosis is characterised by the presence of iron oxide deposits suggesting that iron oxidation may represent an alternative energy-pathway for the bacterial community, especially in shrimps found at the Rainbow site (Gloter et al., 2004; Zbinden et al., 2004; Schmidt et al., 2008). Moreover, the simultaneous occurrence of the bacteria and the iron oxide deposits in
15 the gill chamber of *R. exoculata* may be interpreted as bacterially mediated (Zbinden et al., 2004; Gloter et al., 2004, Anderson et al., 2008).

Several studies have documented the formation and occurrence of iron oxides formed as a result of biotic pathways in natural environments (Fortin et al., 1998; Fortin and Châtellier, 2003; Fortin and Langley, 2005; Banfield et al., 2000; Kennedy et al.,
20 2003, 2004). In this context, the bacteria-hydrous ferric oxide interactions have also been investigated to determine the direct and/or indirect bacterial influence on the hydrous ferric oxide formation (see reviews in Fortin and Langley, 2005; Klapper and Straub, 2005). Some authors (Mavrocordatos and Fortin, 2002; Rancourt et al., 2005) have indicated that bacteria, either iron-metabolizing or non-metabolizing, could influ-
25 ence the mineral deposition. They found evidence of the biogenic origin of the hydrous ferric oxide, identified the presence of poorly crystallized iron oxides, and determined the typical Fe/O ratios and particle size ranges. Natural biogenic iron oxides generally contain impurities, such as adsorbed or structural SiO_2, and phosphate, sulphate, and manganese and aluminium ions, impurities that may influence the spatial organization

and the morphology of the mineral particles (Fortin and Châtellier, 2003; Châtellier et al., 2004). The properties of the iron oxide deposits and the influence of any impurities on these properties have been studied in samples from natural environments (Fortin and Langley, 2005) but have never been investigated in the case of a bacterial ectosymbiosis.

Because the iron oxide deposition could be actively or passively promoted by *R. exoculata* ectosymbiotic bacteria, the main goal of this study is to investigate in detail the structure and the composition of the bacteria-associated mineral particles by using various imaging techniques, such as back-scattered electron imaging, transmission electron microscopy, energy dispersive X-ray microanalysis, and Mössbauer spectroscopy. These investigations have been performed on the fully formed mineral crust of pre-moult shrimps, a crust that is divided into three levels related with the successive steps of formation and growth of the mineral particles.

2 Materials and methods

2.1 Shrimp selection and samples treatment

Specimens of *Rimicaris exoculata* were collected during the French cruise "EXOMAR" (August 2005) at the MAR hydrothermal vent site Rainbow (36°14.0′ N, 2300 m depth) by using the suction sampler of the ROV "Victor 6000" operating from the RV "Atalante." Immediately after retrieval, entire living specimens were either frozen at −80°C or dissected into body parts, branchiostegite and tail, and fixed in a 2.5% glutaraldehyde in seawater 7/10 at pH 7.2 medium.

Observations and analyses were performed on preecdysial specimens, in moult stages D_1''' and D_2, in agreement with the moult-staging method of Drach and Tchernigovteff (1967), based on the development of setae matrices along the uropods borders. The six frozen and four glutaraldehyde-fixed specimens all exhibited an important red-mineral crust on the inner side of the gill chamber (Fig. 1a and b) in agree-

Bacteriogenic iron oxides

L. Corbari et al.

◀ | ▶

◀ | ▶

Back | Close

Full Screen / Esc

Printer-friendly Version

Interactive Discussion

ment with the colour categorisation by Corbari et al. (2008). All the observations were performed on the dorsal median zone of the branchiostegite of *R. exoculata* (Fig. 1a) because it exhibits a regular bacterial and mineral cover that lines the antero-dorsal compartment of the gill chamber (Zbinden et al., 2004). The complete branchiostegite and some portions were photographed with an Olympus SZ40 stereo microscope.

In order to determine the structure and elemental composition of the bacteria-associated minerals, samples were prepared for study by transmission and scanning electron microscopy, X-ray microanalysis, and Mössbauer spectroscopy. During these preparations, contact between air and the samples was avoided to prevent alteration in the oxidation and/or hydration states of the iron oxide minerals. To avoid this air-contact, frozen specimens were used for compositional analyses and compared with glutaraldehyde-fixed specimens. For analytical electron microscopy measurements, the samples, dissected from frozen specimens, were directly dehydrated in absolute ethanol and embedded in epoxy resin (Epofix, Struers) through propylene oxide. Glutaraldehyde-fixed samples, conserved in seawater with NaN_3, were quickly rinsed in distilled water and dehydrated through an ethanol-propylene oxide series of rinses before embedding in the Epofix resin.

2.2 Scanning Electron Microscopy (SEM) and Energy-Dispersive X-ray (EDX) Microanalysis

Polished thin slices of 20 to 50 μm thickness were obtained for the branchiostegites of two glutaraldehyde-fixed and two frozen specimens. The specimens were cut as vertical cross-sections through the mineral crust, i.e., perpendicular to the branchiostegite cuticle. They were polished by abrasion on diamond disks and finally mirror polished with a non-aqueous 1 μm diamond suspension (ESCIL, PS-1MIC). The polished-thin slices were covered with a conductive silver paint, carbon-coated in a Balzers BAF-400 rotary evaporator, and then maintained in desiccators to prevent air-contact before analysis. Structural mineral observations and elemental energy-dispersive X-ray microanalysis were rapidly performed within two days of preparation in an environmental

scanning electron microscope (FEI XL30 ESEM-FEG), operating at 15 to 20 kV and a working distance of 10 mm. A total of 15 polished-thin slices were imaged by back-scattered electrons (BSE) and analysed for the elemental composition of the minerals present.

Elemental analyses have been carried out on the surface of 1 to 2 μm size mineral particles. X-ray microanalyses with an acquisition time of 60 s have been obtained for both the glutaraldehyde-fixed and the frozen samples in order to determine whether any mineral transformation took place through chemical reactions during sample prepara-tion. The elemental quantitative analysis used an automatic background subtraction and a ZAF correction matrix has been used to calculate the elemental composition in weight percents and atomic percents.

2.3 Transmission Electron Microscopy (TEM)

Four glutaraldehyde-fixed specimens were post-fixed in osmium 1%, dehydrated in an ethanol-propylene oxide series and then embedded in epoxy resin (SPI-PON 812). Ultrathin sections were obtained with a Reichert-Jung Ultramicrotome (Ultracut E) by using a diamond knife; uranium acetate and lead citrate were used as contrast agents. The specimens were studied with a Jeol (JEM 100-SX) transmission electron micro-scope operating at 80 kV. In order to provide a three-dimensional view of the mineral crust organisation, vertical cross-sections were cut perpendicular to the branchioste-gite cuticle and the mineral surface and horizontal sections were cut at the three levels of mineral crust as the previously defined.

2.4 Scanning Transmission Electron Microscopy (STEM) and Energy-Dispersive X-ray (EDX) Microanalysis

Ultrathin sections of samples from two frozen shrimps were cut as previously de-scribed, placed on a formvar-coated titanium grid and carbon-coated in a Balzers BAF-400 rotary evaporator. They were then imaged without any additional contrast in a FEI

Tecnai G2 Twin scanning-transmission electron microscope operating at 200 kV.

In order to determine the elemental composition of the strata observed in the mineral particles, scanning transmission electron imaging has been carried out in a both direct bright-field and a high-angle annular dark-field (HAADF) imaging modes. The energy-dispersive X-ray nanoanalyses were performed with a nanoprobe spot size of 1nm in diameter. Profile spectra have been determined on 1 to 1.5 μm length of ten various mineral particles.

2.5 Mössbauer spectroscopy

The Mössbauer spectra have been obtained on samples from frozen shrimps. Two different types of Mössbauer spectral absorbers have been used. The first contained boron nitride mixed with 14 mg/cm^2 of lyophilized powder of crust minerals obtained by scrapings from three shrimps. The second consisted in the superimposed branchiostegites of one shrimp. The spectra were measured between 4.2 and 295 K on a constant-acceleration spectrometer that utilised a room temperature rhodium matrix cobalt-57 source and was calibrated at 295 K with α-iron powder. The estimated relative errors are ±0.005 mm/s for the isomer shifts, ±0.01 mm/s for the quadrupole splittings and line widths, and ca. ±0.5 T for the hyperfine field. The absolute errors are estimated to be approximately twice as large.

2.6 Statistical analysis

The mineralogical compositions and quantifications are reported as mean values ±1 standard deviation. Comparisons of the mineral composition between glutaraldehyde-fixed and frozen samples have been evaluated by using a Mann–Whitney U-test, a two-tailed Student's t-test, a Fisher test, and/or analysis of the variance. $P<0.05$ was taken as the fiducial limit for statistical significance.

3 Results

3.1 Mineral crust ultrastructure

Previously Corbari et al. (2008) have described the formation of a thick mineral crust overlying the bacterial community in the medium zone of the branchiostegites of dark-red shrimps. Three levels in the crust were arbitrarily defined according to the mineral density that gradually increases from the cuticle towards the top surface of the crust. All analysed specimens of *Rimicaris exoculata* exhibit on the inner side of their branchiostegites, a dense, compact, mineral coating with a thickness of up to 100 μm, a mineral coating that corresponds to the mineral crust (Fig. 1a and b). Back scattered electron images of the vertical sections obtained in polished thin slices show the gradual increase in mineral density from the cuticle to the surface of the crust (Fig. 2a, c, and e). In contrast, horizontal ultrathin sections obtained at each of the three identified mineral levels reveal different bacterial densities.

The lower level of the mineral crust (Fig. 2a and b) corresponds to the lower side of the mineral crust and is characterised by a heterogeneous distribution of mineral particles, a distribution that is very fine and seems to correspond to clusters of less than 500 nm size (Fig. 2a). Their morphology seems directly related to the bacterial shape. Transmission electron microscopy images (Fig. 2b) reveal that the lower level is characterised by a high density of rod-shaped bacteria; mineral precipitation occurs on the cell walls of these bacteria (Fig. 3a). The mineral precipitates as individual globular particles of 10 to 30 nm diameter, particles that tend to undergo agglomeration into larger particles. High resolution images (Fig. 3b and c) reveal that the minerals are diffuse and mainly precipitate on secretions of the bacteria, i.e., exopolysaccharides. TEM observations of vertical sections of all the analysed samples reveal that the bacteria form a dense community close to the cuticle, a location in which mineral particles are almost absent because of the probable presence of bacterial secretion (Fig. 4). Interestingly, the methanotrophic bacteria, characterised by their stacks of intracytoplasmic membranes (Fig. 3c), are frequently observed at the lower level of the

crust. Most often they aggregate in isolated groups that remain free of any mineral precipitates (Fig. 3d).

The median level of the crust exhibits larger mineral particles, globular in shape, (Fig. 2c and d). These globular particles often meet to form larger aggregates that appear multiglobular. In the horizontal cross-sections, the mineral density appears rather heterogeneous and consists of highly mineralised patches interspersed with bacteria rich areas. The bacterial density in the median layer is always smaller than in the lower layer; there are fewer rod-shaped bacteria. Moreover, ghosts of bacteria are also observed (Fig. 3e and f) in TEM images. These ghosts have bacterial shapes that are completely enclosed in a heavy mineral sheath. Sometimes the bacteria are still present but appear either to be damaged or as membrane remain (Fig. 3e and f). In other cases, the mineral sheath appears to be empty or to have been recolonised by other rod-shaped bacteria. These observations suggest that mineral formation may influence the survival rate of the bacteria.

The upper level of the mineral crust contains very large particles with diameters of up to $2\,\mu$m (Fig. 2e and f). The "rosette-like" particle shapes with deep indentations suggest that they result from the aggregation of several smaller particles. TEM images reveal that the bacteria become very rare in this upper level. As may be observed in the horizontal sections, almost the only bacteria present are a few large, thin, bacterial filaments that perforate throughout the mineral crust. Moreover, the minerals are not in direct contact with the filament cell walls but form large sheaths at some distance from the cell walls (Fig. 2e). Even though the three step-levels of the mineral crust have been arbitrarily defined, they are representative of the different phases of the mineral formation and are characterised by an inverse correlation, from low to upper levels, between the amount of mineral deposits present and the bacterial density.

3.2 Iron oxides identified by Mössbauer spectroscopy

Mössbauer spectroscopy has been used to identify both the nature and oxidation states of the iron oxides found in the native minerals through the measurements of the iron-

57 isomer shift and quadrupole splitting. The Mössbauer spectra, obtained at 85 and 295 K and between 4.2 and 60 K are shown in Fig. 5a and b, respectively. At 85 and 295 K the spectra consist of broadened quadrupole doublets, whereas below 60 K they consist of a superposition of broadened doublets and sextets. The observed tem-
5 perature dependence of the Mössbauer spectra is typical of small superparamagnetic particles. The spectra have been fit with two symmetric quadruople doublets and one to three magnetic sextets; the average hyperfine parameters are given in Table 1.

The weighted average isomer shift, $<\delta>$, is typical of iron(III) (Shenoy et al., 1978) and spectral analysis indicates that at least 98% of the iron in the mineral crust must
10 be present as iron(III); two percent by spectral area is the approximate detection limit for the presence of any iron(II). The average hyperfine parameters observed at 295 and 4.2 K are typical (Murad et al., 1987) of two-line ferrihydrite. Two-line ferrihydrite, $Fe_5HO_8 4H_2O$, is a poorly crystalline mineral that forms spherical nanoparticles with a diameter of between 2 and 7 nm, a diameter that depends upon both the crystallinity
15 of the material and the presence of impurities. Also for the same reasons, the average hyperfine field observed at 4.2 K may be reduced from 50 to 46.5 T. In the specimens understudy, the average hyperfine field of 47.8 T corresponds to a reasonably well crystallised sample. The blocking temperature, i.e., the temperature at which the absorption areas of the doublets and sextets are equal, is 55±2 K. By using the anisotropy con-
20 stant (Murad et al., 1987) of 4×10^4 J/m^3 for 5 nm $Fe_5HO_8 4H_2O$ particles, an average particle diameter of 5.6 nm is obtained.

3.3 Quantitative X-ray microanalyses

Back-scattered electrons (BSE) images of polished thin slices of frozen specimens provide a detailed map of the mineral particles in the crust. X-ray microanalyses (n=14)
25 performed in ESEM give accurate qualitative and quantitative determinations of the elemental composition of the mineral deposits. These microanalyses reveal the predominance of iron, with a K_α peak at 6.400 keV and a K_β peak at 7.059 keV, and oxygen with a K_α peak at 0.5425 keV, in the mineral crust (Fig. 6). Minor amounts of silicon

with a K_α peak at 1.740 keV, calcium with a K_α peak at 3.690 keV and a K_β peak at 4.012 keV, phosphorus with a K_α peak at 2.013 keV, magnesium with a K_α peak at 1.253 keV, and sulphur with a K_α peak at 2.307 keV, have also been detected. Elemental quantitative analyses yield the weight and atomic percentages of the elements present, see Table 2. In order to determine the relative amount of the iron oxides and other minerals in the deposits, we have assumed that the minor elements, such as Si, Ca, Mg, S, and P, are present in the stoichiometric ratio with oxygen as is found in the mineral forms of SiO_2, $(Ca,Mg)SO_4$, and $(Ca,Mg)_3(PO_4)_2$. The elemental analyses also provide the percentages of elements inherent to the sample preparation as carbon from the carbon-coating of the sample and chlorine and oxygen from the embedding resin. Additional spectra and elemental quantitative analyses have been carried out exclusively on the resin in order to quantify the amount of their content inherent to the sample preparation. After subtracting these peripheral elements by use of the reference spectra of the resin and carbon coating on a pure mineral sample, the percentages of the remaining available oxygen for each mineral form have been calculated as a function of the atomic percentages; the results of these calculations are given in Table 3. In order to obtain the percentages of the different mineral compounds found in the mineral crust, the two major anions, SO_4^{-2} and PO_4^{-3}, have been assumed to be in their most probable forms, i.e., $(Ca,Mg)SO_4$ and $(Ca,Mg)_3(PO_4)_2$. Iron(III) oxides correspond to ca. 85% of the minerals present in the crust, as has been confirmed by Mössbauer spectroscopy. In addition the crusts contain ca. 8% of SiO_2, ca. 3% $(Ca,Mg)SO_4$ and 3% of $(Ca,Mg)_3(PO_4)_2$.

Comparative elemental X-ray microanalyses carried out on 12 polished thin slices of glutaraldehyde-fixed specimens reveal very similar proportions of the minor SiO_2, $(Ca,Mg)SO_4$, and $(Ca,Mg)_3(PO_4)_2$ minerals, a similarity which suggests that these minerals are not solubilised or removed by the aqueous preparation procedure. However, these analyses differ from those of the frozen sample by the Fe/O ratio in the iron oxide, i.e., after the subtraction of the oxygen from the minor minerals, see Table 4, corresponding to an Fe/O ratio of 0.47 in the frozen specimens. In contrast, the Fe/O ap-

proaches 0.60 in the glutaraldehyde-fixed specimens. These measured Fe/O ratios are statistically different as is indicated by a paired t-test which yields t=7.1, $d.f$=11, and P=0.00002. Hence, the atomic percentage of oxygen is lower in the glutaraldehyde-fixed specimens, in which the glutaraldehyde acts as a reducing agent and modifies the iron oxidation state in the mineral particles.

3.4 Structure and composition of the crust minerals

TEM images obtained on Ur/Pb contrasted ultra-thin vertical sections indicate that most of the mineral particles, which have diameters ranging from 200 to 600 nm, exhibit with layered features in the lower level of the crust (Fig. 7a and b). Most of the specimens exhibit a multilayered pattern with a periodicity of a few nanometers, a pattern that suggests that these particles are composed of ca. 5 to 10 successive strata. All of these strata appear as concentric growth layers originating from a unique nucleation centre, as multiglobular rosette-like particles, particles that change their shape and, for the outer particles, follow the outer particle border (Fig. 7b). Neighbouring particles also exhibit layered patterns that may correspond to similar mineral deposition sequences (Fig. 7a). Mineral nucleation and deposition occurs either close to the rod-shaped bacteria walls or in their near-neighbour environment. Several nucleation centres are located close to the same bacteria and the accumulation of strata leads to the aggregation of mineral particles that, as a consequence, exhibit a rosette-like shape (Fig. 7b). STEM-HAADF images of particles from frozen specimens give an inverted mass contrast of the strata. These images reveal the reality of the strata in terms of the changing mineral density and/or the composition within the particles (Fig. 7c and d).

In order to determine the exact nature of these strata, X-ray nanoanalyses have been carried out by STEM along a direction perpendicular to the strata of some particles observed in the ultrathin sections. The experimental procedure for obtaining these line profiles of 1 to 1.5 μm length is based on the acquisition of a sequence of ca. 700 X-ray spectra per line profile. Subsequent data analysis can differentiate different elements through the number of counts that correspond to a given element found along the

line. Figure 8 illustrates a typical elemental profile for iron, oxygen, and silicon along a 1.2 μm line through a stratified mineral particle. The clear lighter coloured strata in Fig. 8a correspond to a higher iron and oxygen content than is found in the dark strata, see Fig. 8b. In spite of a low number of counts, the silicon profile seems to correlate well with those of iron and oxygen. In order to more accurately characterise the nature of the mineral strata, quantitative elemental analyses have been performed at specific points, i.e., points 1, 2, and 3 in Fig. 8a, at well separated strata along the line profile. The results (Table 5) confirm that the iron and oxygen atomic percentages are high at the lighter strata, points 1 and 3, and very low in the dark strata, position 2.

4 Discussion

A multifacitated analysis carried out on the mineral crust of *R. exoculata* reveals a mineral content of 85% iron(III) oxide and 15% of other minerals such as, SiO_2, $(Ca,Mg)SO_4$, and $(Ca,Mg)_3(PO_4)_2$. The Mössbauer spectral results indicate that the iron(III) oxide as two-line ferrihydrite, $Fe_5HO_8 4H_2O$, which is present in small particles of less than 5 nm diameter. A transmission and scanning electron microscopic study of the mineral crust reveals the particles in present in stratified layers suggesting a sequential deposition with alternating layers of differing mineral density and composition. The description of the bacteria-mineral interactions suggests that both biotic and abiotic mineral particles coexist in the *R. exoculata* ectosymbiosis.

4.1 Iron oxides

Mössbauer spectral results have confirmed that the mineral layer which coats the branchiostegite of *Rimicaris exoculata* is mainly composed of a hydrous iron(III) oxide identified as two-line ferrihydrite, $Fe_5HO_8 4H_2O$. These results are in agreement with the conclusions based on transmission electron microscopy-electron energy loss (TEM-EELS) analyses of mineral particles of *R. exoculata* mouth parts (Gloter et al., 2004).

Printer-friendly Version

Interactive Discussion

Further, the particle diameter of 2 to 7 nm obtained from the Mössbauer spectral results is in complete agreement with that obtained by high-resolution electron microscopic images (Gloter et al., 2004). However, although an earlier TEM-EELS analysis (Gloter et al., 2004) indicated a mixture of 55 to 66% iron(III) and 45 to 34% iron(II), only iron(III) has been detected in the Mössbauer spectra of *R. exoculata*. Hence, if it is assumed that limit of detection for iron(II) is 2%, iron(III) represents more than 98% of the total iron present. This difference in the oxidation state of iron may result from the experimental procedure used herein and the glutaraldehyde-fixation used for the TEM-EELS analysis as is discussed below.

Mössbauer spectroscopy utilises bulk samples of the mineral crust and hence, the results are averaged over a rather large number of small particles, in contrast with the results obtained from electron microscopic techniques that are representative of small portions of the samples. Further, there is neither radiation damage nor preparative damage of the absorbers in the Mössbauer spectral experiments. In contrast, exposure to an electron beam can result in atomic displacement, electronic reduction, electron-beam sputtering and/or heating, electrostatic charging, and radiolysis (Egerton et al., 2004). In a recent study using EELS to evaluate the effects of electron beam damage to ferrihydrite, Pan et al. (2006) observed the reduction of iron(III) to iron(II). These results highlight how investigations carried out under high vacuum in a transmission electron microscope may cause substantial and perhaps unsuspected changes to a mineral sample (Michel et al., 2007).

The presence of ferrihydrite as an essential mineral component of the *R. exoculata* crust is a sign of a biogenic origin of the iron oxide deposits. Indeed, the most common extracellular biogenic iron oxides include oxyhydroxides, e.g., goethite, lepidocrocite, akaganeite, and poorly ordered phases, e.g., two-line and six-line ferrihydrite (Cornell and Schwertmann, 2003; Fortin and Langley, 2005). Furthermore, it is commonly accepted that the product of microbial micro-aerobic iron(II) oxidation is often identified as a poorly crystalline ferrihydrite. The observation of two-line ferrihydrite thus supports the hypothesis of the presence of iron-oxidisers among the ectosymbi-

Printer-friendly Version

Interactive Discussion

otic bacterial community of *R. exoculata* (Zbinden et al., 2004) and validates the first observations on bacterial cultures (Cambon-Bonavita, pers. com.). In hydrothermal environments, ferrihydrite has previously been identified because it is commonly inter-mixed with lithoautotrophic iron(II) oxidizing bacteria, bacteria that act as a causative agent in the formation of the ferrihydrite (Emerson and Moyer, 2002; Kennedy et al., 2003; Kennedy et al., 2004; Little et al., 2004). Very few vent animals have been discovered to live in close association with iron oxide deposits. To the best of our knowledge, only the scaly-foot gastropod found in the hydrothermal vents at the Indian Ridge has been shown to exhibit scale-shaped structures, mineralised with iron sulphides on its foot (Goffredi et al., 2003; Waren et al., 2003). These structures are associated with bacteria but an iron isotopic analysis indicates that sulphur and iron in the sclerites originate from hydrothermal fluids rather than from bacteria (Suzuki et al., 2006). Herein, the presence of ferrihydrite in close interaction with hydrothermal metazoan has been discovered for the first time, in the specific case of the vent shrimp *R. exoculata*.

Elemental quantitative analyses have been performed to determine the Fe/O ratio, a ratio that is commonly used as a signature in biogenic iron oxides. Because of the influence of the sample preparation for ultrastructural and elemental analyses, an alternative experimental procedure has been adopted in this study to reduce damage to the samples containing both bacteria and minerals. The samples for mineralogical analyses were frozen until used and were directly dehydrated by ethanol to avoid both air-contact and any aqueous chemical fixation. This procedure is based on the work of Mavrocordatos and Fortin (2002), who investigated the influence of sample preparation on poorly ordered biotic hydrous iron oxide. To assess the impact of sample fixation on the composition of the *R. exoculata* minerals, Fe/O ratios determined through identical procedures have been compared between frozen and glutaraldehyde-fixed samples. The Fe/O ratio of the glutaraldehyde-fixed minerals is significantly different from that of the frozen minerals. Thus sample preparation may modify the oxidation state of iron. The use of glutaraldehyde, a reducing agent, in addition to electron beam damage in TEM-EELS studies can explain the higher percentage of iron(II) reported by

Bacteriogenic iron oxides

L. Corbari et al.

Printer-friendly Version

Interactive Discussion

Gloter et al. (2004) in their mineral samples. The Fe/O ratio in frozen minerals has been measured to be 0.47, after subtraction of the oxygen associated with minor minerals. This value cannot be compared with the Fe/O ratio of 0.33 obtained by Gloter et al. (2004) because both their analytical approach and mineralogical interpretations are quite different from those used herein. In contrast, the calculated Fe/O ratio of 0.47 may be compared with the 0.417 ratio obtained for abiotic ferrihydrite (Mavrocordatos and Fortin, 2002, and references therein). This higher value can be assigned to the bacterial influence and may be considered as evidence for the biogenic origin of iron oxide deposits.

In conclusion, for future research on *R. exoculata* minerals, sample preparation and, more specifically, the drying process and fixation of the biological samples must be accurately delineated because they both influence the surface properties of ferrihydrite and hence, the iron oxidation state and the Fe/O ratio.

4.2 Intrinsic inorganic constituents

Even though ferrihydrite represents the main component of the mineral crust in *R. exoculata*, elemental and quantitative analyses of the mineral particles have revealed the presence of minor elements, such as Si, P, Ca, S, and Mg. These elements are not considered as impurities (Gloter et al., 2004) but rather as intrinsic inorganic constituents or ligands as suggested by Châtellier et al. (2004) because these authors found that their presence during the oxidation process can affect the mineralogy as well as the size and structure of the iron oxide particles. Because of their large surface areas, small particles of natural biogenic iron oxides generally contain adsorbed elements and ions, such as silicate, sulphate, phosphate, and manganese and aluminium cations (Fortin and Châtellier, 2003; Fortin and Langley, 2005). For example, nanoparticles of iron oxyhydroxide formed during the mineralisation process, can adsorb phosphate and silicate ions (Gilbert and Banfield, 2005). The adsorption of elements on ferrihydrite from the surrounding aqueous milieu can affect its subsequent mineral ordering processes. Specifically, adsorption of silicates has been found to inhibit the conversion of ferrihy-

drite to more crystalline iron oxides, such as hematite and goethite (Kennedy et al., 2003; Châtellier et al., 2004). X-ray nanoanalyses and elemental profiles performed on stratified *R. exoculata* mineral particles have revealed that silicates are already present in the early stages of mineral development. Thus, in *R. exoculata*, it is evident that
inorganic ligands co-precipitate with iron oxide and are closely associated with it in the nanoparticles because the silicate portion cannot be located separately from the iron oxide even on the nanometric scale reached in STEM. In the global characterisation of the mineral particles, we have assumed that they correspond to separated minerals such as silica, $(Ca,Mg)_3(PO_4)_2$, and $(Ca,Mg)SO_4$, even though it is very probable that
silicate, sulphate, phosphate, and magnesium and calcium cations are complexed with ferrihydrite and influence or stabilise this poorly crystalline form of iron oxide. The high silica content of ca. 8% found in the *R. exoculata* mineral crusts presumably result from the silicon concentration in the vent fluid, specifically the 6.9 mM concentration at the Rainbow site (Schmidt et al., 2007) a conclusion that as is also supported by com-
parison with the minerals found in the TAG shrimps (Corbari and Compère, personal communication).

In order to further assess the distribution of the intrinsic inorganic constituents, X-ray spectra acquired at line profiles have been performed on mineral particles exhibiting stratified features. At the atomic level, the results indicate that both iron and the other
inorganic ligands are already associated within nanosized mineral particles. These observations reveal that iron, oxygen, and silicon proportions are constant but that the stratification is mainly the consequence of parallel variations of the concentration of all the constituting elements. We can therefore consider the iron oxide globular particles rather like mineral concretions. Bacteria-associated mineral concretions appear
to be identical and stratification seems to follow the same sequence within neighbouring mineral particles. These observations suggest that micro-environmental variations can occur in the nearby environment during the formation of the mineral particles. Homogenous patterns of stratification on neighbouring particles can be explained by either environmental variations found at the shrimp growth level or by variations in the

bacterial metabolism or activities. Similar patterns of stratification have been previously described on sediment microfacies and delineated as microstromatolite (Boulvain et al., 2001). The "microstromatolite" aspect of the mineral concretions in *R. exoculata* provides one more argument in favour of the biogenic origin of the iron oxides.

4.3 Bacteria-mineral interactions

In *R. exoculata*, iron oxide is complexed with intrinsic inorganic ligands in the presence of an important bacterial community. Both bacteria and the intrinsic inorganic ligands may play a role in mineral deposition. The term of biogenic iron oxides is commonly used to refer to iron oxide formed in the presence of bacteria. It also includes iron oxides formed as a direct result of microbial metabolism, i.e., through enzyme activities, or by passive mechanisms through which bacterial secretions trigger the formation and precipitation of iron oxides minerals (Fortin and Châtellier, 2003).

In *R. exoculata*, mineral deposition only occurs when the bacterial community is well-developed on the inner side of the branchiostegite (Corbari et al., 2008). This observation both contradicts the idea that iron oxide deposition could only result from a passive chemical-induced precipitation and supports the idea that bacteria must participate in mineral formation. Ferrihydrite formed in the absence of bacteria may be metastable and, typically after few days, must transform into a more structurally ordered iron oxide, such as hematite or goethite (Cornell and Schwertmann, 2003). Experiments performed on bacteriogenic ferrihydrite minerals obtained from the hydrothermal vents in the Axial Volcano, in the Pacific Ridge, demonstrated that even if they were subjected to heating of up to 80°C, these minerals did not undergo a phase transition, and therefore suggesting that the presence of bacteria inhibited the ferrihydrite transformation (Kennedy et al., 2004). Hence, the presence of ferrihydrite deposits inside the gill chamber of *R. exoculata* appears to result from the presence of an abundant bacterial community. If the moult cycle is used as a time-scale, the first ferrihydrite deposits are only observed when the bacterial density reaches a maximum in the early preecdysial individuals, i.e., the light-red or medium-red individuals, in stages D_0 to D_1 (Corbari et

al., 2008). During the ten day moult cycle of the vent shrimp, the first mineral parti-
cles appear as ferrihydrite (Corbari and Compère, unpublished data) as early as the
second post-moult day and continue to deposit until the tenth day, just before exuvia-
tion. Hence, we conclude that the bacterial community contributes of the stabilisation
of the iron oxide in the form of ferrihydrite. The bacteria organic moieties can hinder its
transformation into a more crystallized iron oxide (Kennedy et al., 2004) or favour the
incorporation of the minor ligands.

TEM observations of the bacterial morphotypes and their mineral interactions help
to elucidate the biogenic origin of the ferrihydrite deposits inside the gill chamber of
R. exoculata. Different ways of mineral deposition have been identified, based on the
recurrent observations of both bacterial morphotypes and mineral morphologies. Two
association modes between minerals and rod shaped bacteria have been observed. In
the first, iron oxide deposition occurs in close contact to the rod cell walls and, in the
second, the iron oxide precipitates on polysaccharide or proteinaceous extracellular
secretions at a significant distance from the bacterial cells. Such bacterial-mineral
relationships have previously been described, suggesting that rods are mainly involved
in iron oxide formation (Anderson et al., 2008). The precipitation of iron oxides on or
near the bacterial cell walls raises the question: Is it possible to determine whether
the ectosymbiotic bacteria found in the gill chamber of *R. exoculata* are actively or
passively depositing iron oxide minerals?

Passive reactions linked to biogenic iron oxide production are related to the reactivity
of the bacterial cell walls. Mineral formation on the bacteria is generally not controlled
by the organism but, rather, it results from the chemistry of the cell environment and
the physicochemistry of the bacterial surface, (Fortin and Langley, 2005) a result that
implies the adsorption and/or nucleation of iron oxide particles on bacterial cell walls
(Fortin and Châtellier, 2003). Whatever types of cell surface structure the cell may
have, the main charged chemical constituents found in these structures at neutral pH
are carboxyl, phosphoryl, and amino groups (Douglas and Beveridge, 1998). We thus
suspect that similar mineral-bacteria associations take place in *R. exoculata* and that

there is passive deposition of iron oxides. In addition, it is unclear whether precipitation of iron(III) minerals in close vicinity of the cells, or even at the cell surface, is harmful for the cells as a result of limiting substrate diffusion and uptake, as is commonly assumed (Hallberg and Ferris, 2004). The observed ghosts of bacteria surrounded by a dense mineral coating suggest that these bacteria are probably not iron-oxidising bacteria because deposition of heavy minerals on their cell walls should improve their survival rate.

The active metabolic processes of iron oxidation in iron metabolizing bacteria have to be distinguished from the indirect biologically induced iron oxide deposition in which the bacterial cell surface simply acts as a passive deposition template (Konhauser, 1997; Klapper and Straub, 2005). The most studied iron-oxidising bacteria are the neutrophilic aerobic iron(II) oxidisers from *Gallionella* and *Leptothrix* genus, oxidisers that produce extracellular organic polymers that nucleate iron(III) precipitates. It has been suggested that these microbes use these strategies to avoid encrustation of the metabolising cells that would lead to impaired substrate uptake and metabolite release, and might even cause cell death (Hallberg and Ferris, 2004; Kappler et al., 2005). Hence, if iron-oxidizing bacteria are present among the ectosymbiotic community in *R. exoculata*, they could use this strategy to keep their metabolism active and only those with extracellular secretion would be involved in iron oxide formation. The presence of a mineral boundary between the dense rod population and the mineralised area suggests a strategy involving the production of an extracellular organic material in order to prevent mineral deposition directly on the bacterial cell walls. Finally, the weak mineral deposition, maximal rod-shaped bacterial density, and presence of extracellular secretions suggest that iron-oxidising bacteria may be located in this layer, a layer that may act as a potential reserve for active ectosymbiotic bacteria.

Interestingly, the appearance of methanotrophic bacteria clusters also support the above described mechanism in which bacteria exude organic substances to prevent any mineral deposition directly on their cell walls. Further, the presence of methanotrophic bacteria suggests a more diversified bacterial community than previously men-

tioned (Segonzac et al., 1993; Zbinden et al., 2004; Corbari et al., 2008). Herein, methanotrophic bacteria show intact internal structures, i.e., stalks, and are distributed in clusters that indicate an active metabolism.

The three step-levels in the mineral crust formation previously described (Corbari et al., 2008) indicates that iron oxide particle growths are continuously initiated from the lower level, in close association with growing bacteria and subsequently grow into the median and upper levels. The mineralisation within the gill chamber could be described as a dynamic process in which particles increase in size and are simultaneously pushed upward by the formation of new particles. As has been illustrated herein, the lower level exhibits the highest bacterial density and is mainly composed of rod bacteria. This level may be considered as a bacterially active layer and its evolution in time, based on the moult cycle, shows continuous growth (Corbari et al., 2008).

5 Conclusions

The multidisciplinary approach used in the present study provides new details about the iron oxide deposits associated with ectosymbiotic bacteria in *Rimicaris exoculata*. The mineral crust has been identified as a dense layer of two-line ferrihydrite nanoparticles intermixed with other intrinsic inorganic constituents, mainly SiO_2. Various investigations on these nanoparticles have revealed that these minerals all contribute to the mineral particles deposited in the gill chamber. Their subtraction from the concretion composition has led to an of Fe/O ratio of 0.47 in the remaining ferrihydrite, a ratio that suggests a bacteriogenic origin for the ferrihydrite. More morphological evidence has been obtained that determines the role of bacterial morphotypes in the "active" deposition of iron oxides. The process of mineralisation in the gill chambers of *R. exoculata* remains complex because the combined effects of the intrinsic inorganic constituents and the bacterial cells is difficult to disentangle. But the evolution of the bacterial density in the three levels of the mineral crust is closely related to the amount of iron deposited and it is proposed that the lower level is the likely region where the

iron-oxidising bacteria are located. But the presence of a more diversified bacterial community raises the question on the metabolic or genetic diversity of these bacteria.

Because the main studies on *R. exoculata* ectosymbiosis have been performed on shrimps from the vent site Rainbow, the influence of the chemical vent environment should be studied in the future by comparing ectosymbiosis and its associated minerals in *R. exoculata* specimens collected at different vent sites, for instance TAG, Logatchev, and Snake Pit. This indirect approach could be used to evaluate how representative is the *R. exoculata* ectosymbiosis and, thus to determine whether iron oxidation represents the most favourable energetic-pathways for ectosymbiotic bacteria (Schmidt et al., 2008).

References

Anderson, L., Halary, S., Lechaire, J.-P., Boudier, T., Frebourg, G., Marco, S., Zbinden, M., and Gaill, F.: Tomography of bacteria-mineral associations within the deep-sea hydrothermal vent shrimp rimicaris exoculata, Comptes Rendus Chimie, 11, 268–280, 2008.

Banfield, J. F., Welch, S. A., Zhang, H., Ebert, T. T., and Penn, L. P.: Aggregation-based crystal growth and microstructure development in natural iron oxyhydroxide biomineralization products, Science, 289, 751–754, 2000.

Boulvain, F., De Ridder, C., Mamet, B., Préat, A., and Gillan, D.: Iron microbial communities in belgian frasnian carbonate mounds, Facies, 44, 47–60, 2001.

Bacteriogenic iron oxides

L. Corbari et al.

Casanova, B., Brunet, M., and Segonzac, M.: L'impact d'une épibiose bactérienne sur la mor-phologie fonctionnelle de crevettes associées à l'hydrothermalisme médio-atlantique, Cah. Biol. Mar., 34, 573–588, 1993.

Cavanaugh, C., McKiness, Z., Newton, I., and Stewart, F.: Marine chemosynthetic symbioses, in: The prokaryotes, edited by: Dworkin, M., Falkow, S., Rosenberg, E., Schleifer, K., and Stackebrandt, E., Springer, New York, 475–507, 2006.

Châtellier, X., Fortin, D., West, M., Leppard, G., and Ferris, F.: Effect of the presence of bacterial surfaces during the synthesis of fe-oxides by oxidation of ferrous ions, Eur. J. Miner., 13, 705–714, 2001.

Châtellier, X., West, M. M., Rose, J., Fortin, D., Leppard, G. G., and Ferris, F. G.: Characteri-zation of iron-oxides formed by oxidation of ferrous ions in the presence of various bacterial species and inorganic ligands, Geomicrobiol. J., 21, 99–112, 2004.

Corbari, L., Zbinden, M., Cambon-Bonavita, M.-A., Gaill, F., and Compère, P.: Bacterial sym-bionts and mineral deposits in the branchial chamber of the hydrothermal vent shrimp *Rimi-caris exoculata*: Relationship to moult cycle, Aquatic Biology, 1, 225–238, 2008.

Cornell, R. and Schwertmann, U.: The iron oxides – structure, properties, occurrences and uses, 2nd edition, Weinheim ed., Wiley-VCH Verlag, 664 pp., 2003.

Desbruyeres, D., Biscoito, M., Caprais, J.-C., Colaco, A., Comtet, T., Crassous, P., Fouquet, Y., Khripounoff, A., Le Bris, N., and Olu, K.: Variations in deep-sea hydrothermal vent communi-ties on the Mid-Atlantic Ridge near the Azores plateau, Deep-sea Res. PtI, 48, 1325–1346, 2001.

Douglas, S. and Beveridge, T. J.: Mineral formation by bacteria in natural microbial communi-ties, FEMS Microbiol. Ecol., 26, 79–88, 1998.

Drach, P. and Tchernigovtzeff, C.: Sur la méthode de détermination des stades d'intermue et son application générale aux crustacés, Vie et Milieu, 18, 595–609, 1967.

Edwards, K. J., Bach, W., McCollom, T. M., and Rogers, D. R.: Neutrophilic iron-oxidizing bac-teria in the ocean: Their habitats, diversity, and roles in mineral deposition, rock alteration, and biomass production in the deep-sea, Geomicrobiol. J., 21, 393–404, 2004.

Egerton, R. F., Li, P., and Malac, M.: Radiation damage in the TEM and SEM, Micron, 35, 399–409, 2004.

Emerson, D. and Moyer, C. L.: Neutrophilic Fe-oxidizing bacteria are abundant at the Loihi seamount hydrothermal vents and play a major role in Fe oxide deposition, Appl. Environ. Microb., 68, 3085–3093, 2002.

Bacteriogenic iron oxides

L. Corbari et al.

Title Page

Abstract	Introduction
Conclusions	References
Tables	Figures

|◄ | ►|

◄ | ►

Back | Close

Full Screen / Esc

Printer-friendly Version

Interactive Discussion

Fortin, D., Ferris, G., and Scott, S.: Formation of Fe-silicates and Fe-oxides on bacterial surfaces in samples collected near hydrothermal vents on the southern explorer ridge in the northeast Pacific ocean, American Mineralogist, 83, 1399–1408, 1998.

Fortin, D. and Châtellier, X.: Biogenic iron-oxides, Recent Research Developments in Mineralogy, 3, 47–63, 2003.

Fortin, D. and Langley, S.: Formation and occurrence of biogenic iron-rich minerals, Earth-Sci. Rev., 72, 1–19, 2005.

Gebruk, A., Pimenov, N., and Savvichev, A.: Feeding specialization of bresiliid shrimps in the tag site hydrothermal community, Mar. Ecol.-Prog. Ser., 98, 247–253, 1993.

Gebruk, A. V., Southward, E. C., Kennedy, H., and Southward, A. J.: Food sources, behaviour, and distribution of hydrothermal vent shrimps at the mid-atlantic ridge, J. Mar. Biol. Ass. UK, 80, 485–499, 2000.

Gilbert, B. and Banfield, J. F.: Molecular-scale processes involving nanoparticulate minerals in biogeochemical systems, Rev. Mineral. Geochem., 59, 109–155, 2005.

Gloter, A., Zbinden, M., Guyot, F., Gaill, F., and Colliex, C.: TEM-EELS study of natural ferrihydrite from geological-biological interactions in hydrothermal systems, Earth Planet. Sci. Lett., 222, 947–957, 2004.

Goffredi, S., Hurtado, L., Hallam, S., and Vrijenhoek, R.: Evolutionary relationships of deep-sea vent and cold seep clams (mollusca: Vesicomyidae) of the "Pacifica/lepta" Species complex, Marine Biology, 142, 311–320, 2003.

Hallberg, R. and Ferris, F. G.: Biomineralization by *Gallionella*, Geomicrobiol. J., 21, 325–330, 2004.

Kappler, A., Schink, B., and Newman, D. K.: Fe(III) mineral formation and cell encrustation by the nitrate-dependent Fe(II)-oxidizer strain bofen1, Geobiology, 3, 235–245, 2005.

Kappler, A. and Straub, K. L.: Geomicrobiological cycling of iron, Rev. Mineral. Geochem., 59, 85–108, 2005.

Kennedy, C. B., Martinez, R. E., Scott, S., and Ferris, F. G.: Surface chemistry and reactivity of bacteriogenic iron oxidesfrom axial volcano, juan de fuca ridge, north-east pacific ocean., Geobiology, 1, 59–69, 2003.

Kennedy, C. B., Scott, S. D., and Ferris, F. G.: Hydrothermal phase stabilization of 2-line ferrihydrite by bacteria, Chem. Geol., 212, 269–277, 2004.

Konhauser, K. O.: Bacterial iron biomineralisation in nature, FEMS Microbiol. Rev., 20, 315–326, 1997.

Little, C., Glynn, S., and Mills, R. A.: Four-hundred-and-ninety-million-year record of bacteriogenic iron oxide precipitation at sea-floor hydrothermal vents, Geomicrobiol. J., 21, 415–429, 2004.

Mavrocordatos, D. and Fortin, D.: Quantitative characterization of iron oxides formed on bacterial walls by tem-eels, Am. Miner., 87, 940–946, 2002.

Michel, F. M., Ehm, L., Antao, S. M., Lee, P. L., Chupas, P. J., Liu, G., Strongin, D. R., Schoonen, M. A. A., Phillips, B. L., and Parise, J. B.: The structure of ferrihydrite, a nanocrystalline material, Science, 316, 1726–1729, 2007.

Murad, E. and Johnston, J. H.: Mössbauer spectroscopy applied to inorganic chemistry, edited by: Long, G. J., Plenum Press New York, 507 pp., 1987.

Murad, E. and Schwertmann, U.: Iron oxide mineralogy of some deep-sea ferromanganese crusts, Am. Miner., 73, 1395–1400, 1988.

Page, H. M., Fisher, C. R., and Childress, J.: The role of suspension-feeding in the nutritional biology of a deep-sea mussel with methanotrophic symbionts, Mar. Biol., 104, 251–257, 1990.

Pan, Y., Brown, A., Brydson, R., Warley, A., Li, A., and Powell, J.: Electron beam damage studies of synthetic 6-line ferrihydrite and ferritin molecule cores within a human liver biopsy, Micron, 37, 403–411, 2006.

Polz, M. F. and Cavanaugh, C. M.: Dominance of one bacterial phylotype at a Mid-Atlantic Ridge hydrothermal vent site, PNAS, 92, 7232–7236, 1995.

Polz, M. F., Robinson, J. J., Cavanaugh, C. M., and Van Dover, C. L.: Trophic ecology of massive shrimp aggregations at a mid-atlantic ridge hydrothermal vent site, Limnol. Oceanogr., 43, 1631–1638, 1998.

Pond, D., Bell, M., Dixon, D., and Sargent, J.: Occurrence of 16:2(n-4) and 18:2(n-4) fatty acids in the lipids of the hydrothermal vent shrimp *Rimicaris exoculata*: Nutritional and trophic implications, Mar. Ecol.-Prog. Ser., 156, 167–174, 1997.

Rieley, G., Dover, C. L. V., Hedrick, D. B., and Eglinton, G.: Trophic ecology of *Rimicaris exoculata*: A combined lipid abundance/stable isotope approach, Mar. Biol., 133, 495–499, 1999.

Schmidt, C., Vuillemin, R., Le Gall, C., Gaill, F., and Le Bris, N.: Geochemical energy sources for microbial primary production in the environment of hydrothermal vent shrimps, Mar. Chem., 108, 18–31, 2008.

Schmidt, K., Koschinsky, A., Garbe-Schonberg, D., de Carvalho, L. M., and Seifert, R.: Geo-

chemistry of hydrothermal fluids from the ultramafic-hosted logatchev hydrothermal field, 15° N on the Mid-Atlantic Ridge: Temporal and spatial investigation, Chem. Geol., 242, 1–21, 2007.

Segonzac, M., de Saint-Laurent, M., and Casanova, B.: L'énigme du comportement trophique des crevettes Alvinocarididae des sites hydrothermaux de la dorsale Médio-Atlantique, Cah. Biol. Mar., 34, 535–571, 1993.

Shenoy, G. K., Wagner, F. E., and Kalvius, G. M.: Mössbauer isomer shifts, edited by: Shenoy, G. K. and Wagner, F. E., North-Holland Amsterdam, 49 pp., 1978.

Suzuki, Y., Kopp, R. E., Kogure, T., Suga, A., Takai, K., Tsuchida, S., Ozaki, N., Endo, K., Hashimoto, J., Kato, Y., Mizota, C., Hirata, T., Chiba, H., Nealson, K. H., Horikoshi, K., and Kirschvink, J. L.: Sclerite formation in the hydrothermal-vent "Scaly-foot" Gastropod-possible control of iron sulfide biomineralization by the animal, Earth Planet. Sci. Lett., 242, 39–50, 2006.

Van Dover, C., Fry, B., Grassle, F., Humphris, S., and Rona, P. A.: Feeding biology of the shrimp *Rimicaris exoculata* at hydrothermal vents on the mid-atlantic ridge., Mar. Biol., 98, 209–216, 1988.

Warén, A. S., Bengtson, S. K., Goffredi, S., and Van Dover, C. L.: A hydrothermal-vent gastropod with iron sulfide biomineralized dermal sclerites, Science, 302, 1007, 2003.

Williams, A. and Rona, P. A.: Two new caridean shrimps (bresiliidae) from a hydrothermal field on the mid-Atlantic Ridge., J. Crustac. Biol., 6, 446–462, 1986.

Wirsen, C. O., Jannasch, H. W., and Molyneaux, S.: Chemosynthetic microbial activity at Mid-Atlantic Ridge hydrothermal vent sites, J. Geophys. Res., 98, 9693–9703, 1993.

Zbinden, M. and Cambon-Bonavita, M.-A.: Occurrence of deferribacterales and entomoplasmatales in the deep-sea alvinocarid shrimp *Rimicaris exoculata* gut, FEMS Microbiol. Ecol., 46, 23–30, 2003.

Zbinden, M., Le Bris, N., Gaill, F., and Compère, P.: Distribution of bacteria and associated minerals in the gill chamber of the vent shrimp *Rimicaris exoculata* and related biogeochemical processes, Mar. Ecol.-Prog. Ser., 284, 237–251, 2004.

Table 1. Mössbauer spectral parameters obtained for the *Rimicaris exoculata* hydrothermal shrimp. [a]The isomer shifts are given relative to room temperature α-iron powder.

Compound	T, K	$<\delta>$, mm/s[a]	$<\Delta E_Q>$, mm/s	$<H>$, T	$<\Gamma>$, mm/s	Area, %	Abs. Area, (%ε)(mm/s)	Assignment
Rainbow	295	0.358	0.78	0	0.46	100	7.302	Superparamagnetic iron(III)
	225	0.403	0.78	0	0.38	100	10.106	Superparamagnetic iron(III)
	155	0.439	0.79	0	0.39	100	11.010	Superparamagnetic iron(III)
	85	0.465	0.80	0	0.42	100	11.064	Superparamagnetic iron(III)
	60	0.464	0.80	0	0.42	82	6.196	Superparamagnetic iron(III)
		0.461	-0.04	39.6	1.13	18	1.314	Partially blocked iron(III)
	50	0.464	0.80	0	0.42	36	3.6935	Superparamagnetic iron(III)
		0.463	-0.05	21.6	4.35	64	6.693	Partially blocked iron(III)
	45	0.464	0.80	0	0.42	23	2.332	Superparamagnetic iron(III)
		0.463	-0.06	28.1	3.54	77	7.753	Partially blocked iron(III)
	40	0.464	0.80	0	0.42	8	0.901	Superparamagnetic iron(III)
		0.463	-0.06	24.0	3.75	92	10.075	Partially blocked iron(III)
	4.2	0.481	-0.045	47.8	0.56	100	10.727	Blocked iron(III)

Table 2. Typical elemental X-ray microanalysis of the mineral crust of *Rimicaris exoculata*. Data are expressed as both weight and atomic percents.

Element	Wt %	At %
C K	37.5	57.3
O K	25.5	29.2
MgK	0.4	0.3
SiK	1.7	1.1
P K	0.6	0.3
S K	0.3	0.2
ClK	0.3	0.2
CaK	0.6	0.3
FeK	32.7	10.8

Table 3. Mineralogical characterisation of the mineral crust in *Rimicaris exoculata*. Data are expressed in atomic percentages and results from elemental quantitative analyses of polished thin slices of minerals taken from two frozen specimens. Mean values have been calculated after removing the peripheral elements inherent to the resin and the carbon coating. The amount of available oxygen is calculated assuming the presence of the SO_4^{-2} and PO_4^{-3} anionic groups. The percentages of mineral compounds have been calculated under the assumption of the most probable mineral occurrence. All values are averages ±1 standard deviation.

Elements	O	Fe	Si	S	P	Ca	Mg
Mean	67.8 ± 1.4	27.3 ± 0.7	2.6 ± 0.4	0.5 ± 0.1	0.5 ± 0.2	0.7 ± 0.1	0.5 ± 0.3
Available O	-	58.5 ± 3.1	5.3 ± 0.8	2.1 ± 0.4	2.0 ± 0.9	-	-
Anionic groups				SO_4^{2-} 2.6 ± 0.5	PO_4^{2-} 2.5 ± 1.2		
Mineral compounds		$Fe_xO_y(OH)_z+vH_2O$ 85.8 ± 2.9	SiO_2 7.9 ± 1.2	$(Ca,Mg)SO_4$ 3.1 ± 0.6	$(Ca,Mg)_3(PO4)_2$ 3.2 ± 1.5		Total 99.9 ± 0.2

Table 4. Comparison of the mineralogical composition between frozen and glutaraldehyde fixed specimens. X-ray elemental quantitative analysis of fourteen frozen samples and twelve glutaraldehyde-fixed samples. The data have been obtained with the same experimental procedure. All values are means ±1 standard deviation. * means significantly different.

Elements	Frozen sp.		Glutharaldehyde-fixed sp.	
	O	Fe	O	Fe
Mean	67.8 ± 1.4	27.3 ± 0.7	64.5 ± 1.4	28.3 ± 1.3
Available O	-	58.5 ± 3.1	-	47.8 ± 3.0
Ratio Fe/O	0.47 ± 0.03		0.60 ± 0.05 *	

Table 5. Elemental quantitative analyses expressed in atomic percent along the line profile of the iron oxide particle shown in Fig. 8a. Positions 1, 2, and 3 correspond to the positions indicated in Fig. 8a.

% At	Fe(K)	O(K)	Si(K)
1	4.62	10.95	0.55
2	1.07	4.57	0.34
3	1.99	6.54	0.36

Fig. 1. *Rimicaris exoculata*. **(a)** Inner side of the branchiostegite (left side) of premoult specimen in moult stage D1‴ exhibiting a dense and uniform coating of mineral deposits. The dashed lines delimit the observed area, the median zone. **(b)** Polished thin cross section slices of the mineral crust observed under a light microscope and exhibiting three different layers of mineral density. Note that the bacterial filaments are distinguishable on the upper level of the picture.
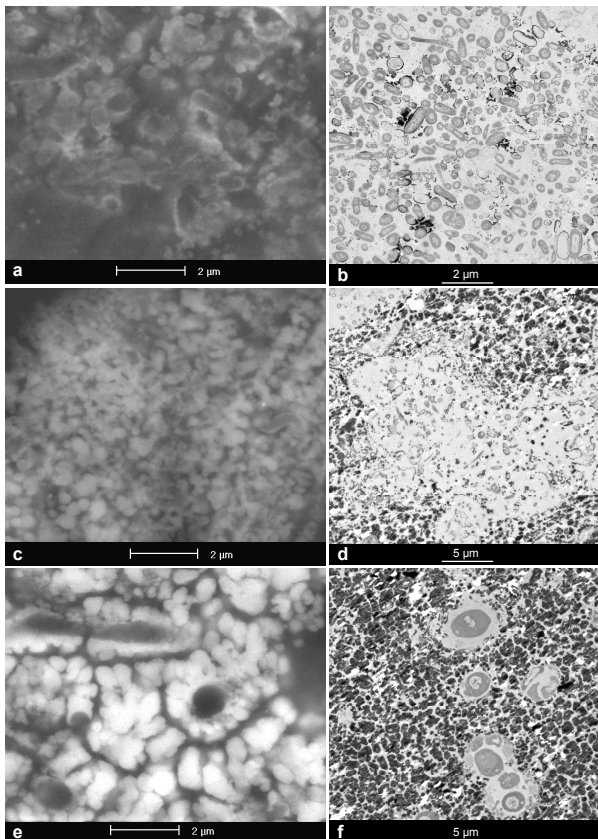
Fig. 2. The three levels of the mineral crust. Comparison between the electron back scattering images of the polished-thin sections (vertical sections) revealing the mineral densities and structures (left column) and the TEM micrographs of horizontal cross-sections exhibiting mineral associated with bacterial community (right column) at the lower level (**a** and **b**), the median level (**c** and **d**) and the upper level (**e** and **f**).
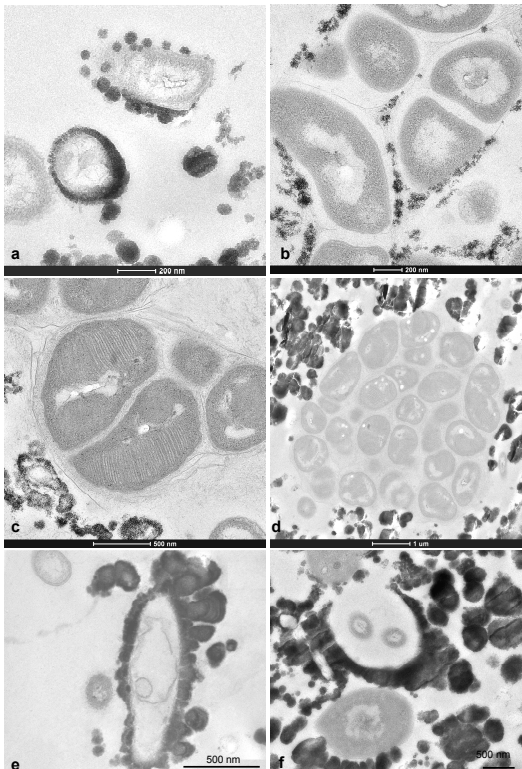
Fig. 3. TEM views illustrating the different ways the minerals may be deposited on the rod-shaped bacteria in *Rimicaris exoculata*. **(a)** Mineral deposition in direct contact with the bacteria cell walls. **(b)** Mineral deposition on secreted bacterial substance. (**c** and **d**) Methanotrophic bacteria surrounded by mineral deposits. (**e** and **f**) Bacterial ghosts coated with minerals and bacterial recolonization of the mineral sheaths.

2 µm
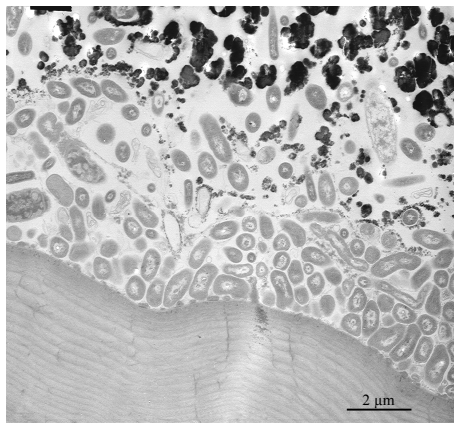
Fig. 4. Bacteria-mineral interactions in *Rimicaris exoculata*. TEM view of the lower level (vertical cross-section) where rod-shape bacteria are very abundant. Note that the bacteria seem to produce some substance which prevents any direct mineral deposition close to this layer.
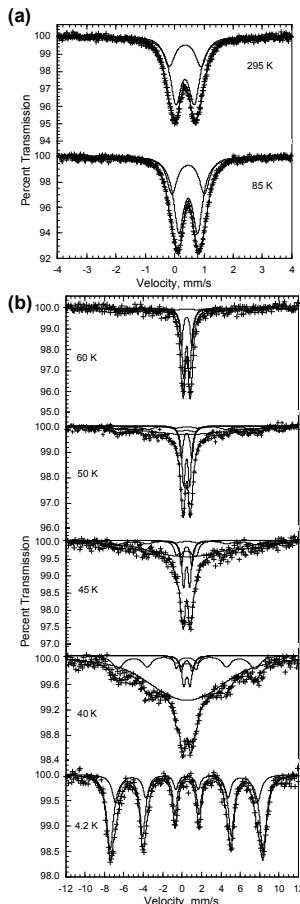
Fig. 5. **(a)** The 85 and 295 K iron-57 Mössbauer spectra of minerals from the crust collected on the branchiostegites of three shrimps. **(b)** The iron-57 Mössbauer spectra of two superimposed branchiostegites parts of one shrimp obtained at the indicated temperatures.

Bacteriogenic iron oxides

L. Corbari et al.
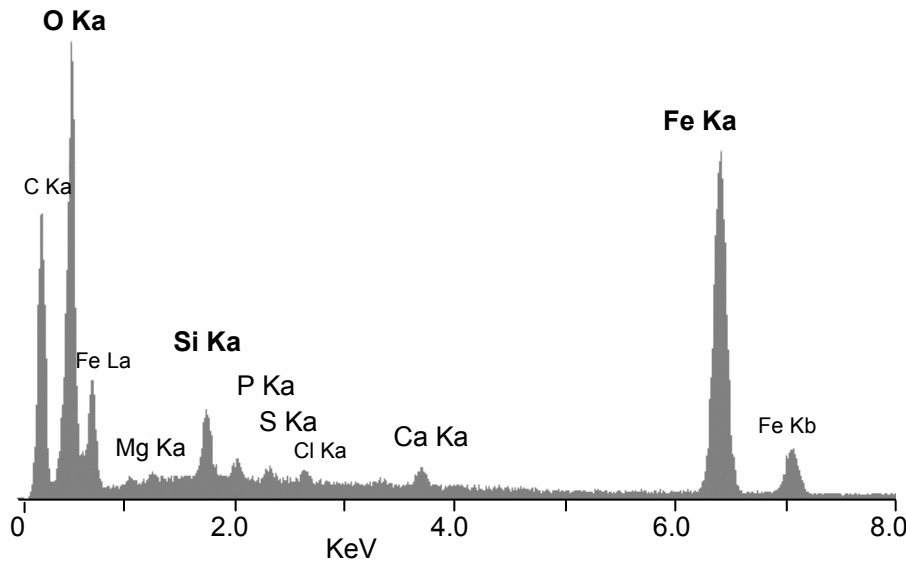
Fig. 6. Elemental X-ray microanalyses of the mineral crust of *Rimicaris exoculata*. **(a)** A typical spectrum obtained on mineral particles of up to $2\,\mu$m diameter. The peaks are labelled with the X-ray line of the corresponding element.

Title Page

Abstract | Introduction

Conclusions | References

Tables | Figures

◄ | ►►

◄ | ►

Back | Close

Full Screen / Esc

Printer-friendly Version

Interactive Discussion
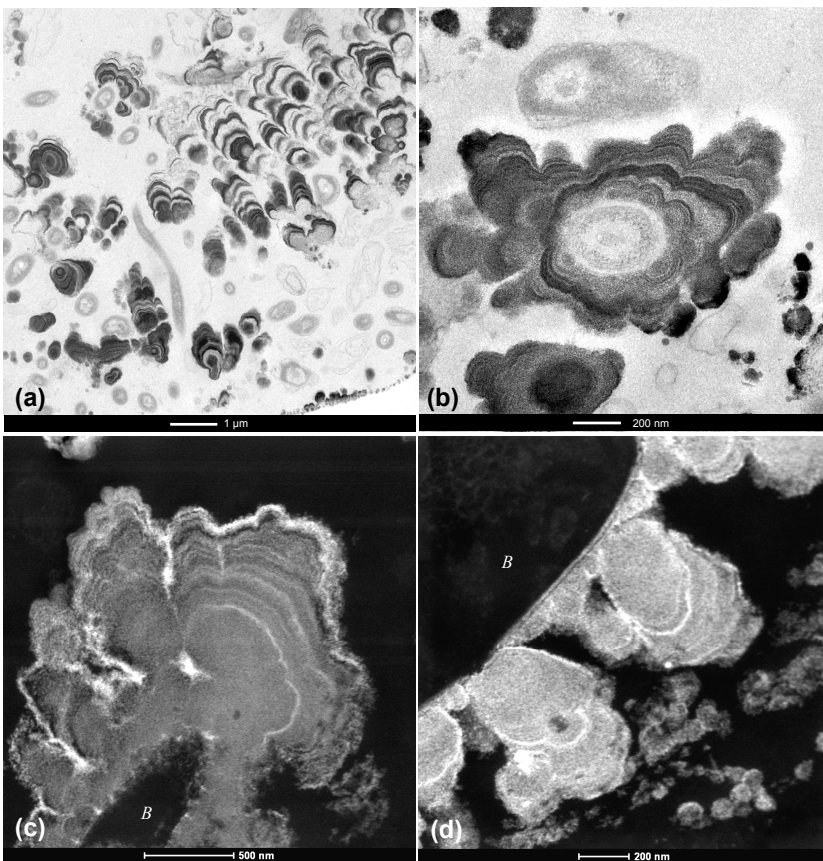
Fig. 7. (**a** and **b**) TEM views of the mineral particles in the lower level of the crust. The occurrence of contrasted strata is clearly visible. (**c** and **d**) STEM images of ultrathin sections of non-contrasted mineral particles revealing the different nature of the mineral strata. *B* indicates the bacteria.
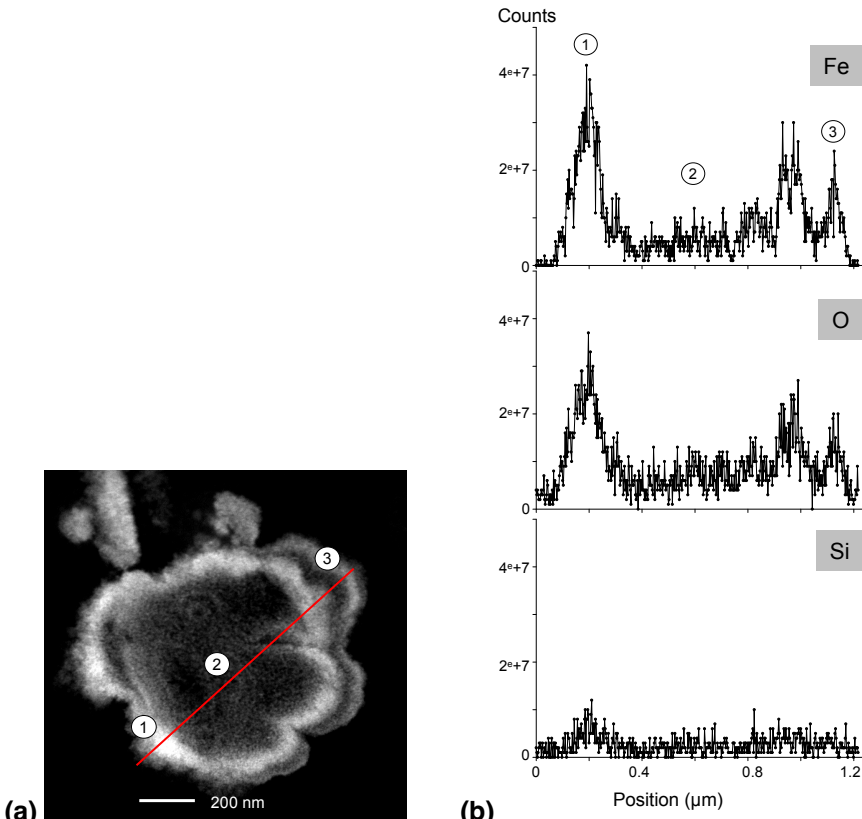
Fig. 8. (a) STEM pictures of the analysed particle exhibiting contrasted strata. The red line corresponds to the spectral profile line of $1.2\,\mu m$ length. The numbers 1 to 3 indicate the points where the elemental quantitative analysis given in Table 5 was carried out. **(b)** Element specific spectra acquired along the red profile line. Points 1 to 3 are also indicated at their corresponding positions on the iron spectrum.